JCTC Journal of Chemical Theory and Computation

Article

pubs.acs.org/JCTC

Excited State Geometries and Vertical Emission Energies of Solvated Dyes for DSSC: A PCM/TD-DFT Benchmark Study

Caterina Bernini,[†,#] Lorenzo Zani,[‡] Massimo Calamante,[‡] Gianna Reginato,[‡] Alessandro Mordini,[‡] Maurizio Taddei,[†] Riccardo Basosi,[†,#] and Adalgisa Sinicropi*[,†,#]

[†]Dipartimento di Biotecnologie, Chimica e Farmacia, Università di Siena, Via A. Moro 2, 53100 Siena, Italy

[‡]CNR − Istituto di Chimica dei Composti Organometallici (CNR-ICCOM), Via Madonna del Piano 10, 50019 Sesto Fiorentino, Florence, Italy

[#]CSGI, Consorzio per lo Sviluppo dei Sistemi a Grande Interfase, via della Lastruccia 3, 50019 Sesto Fiorentino, Florence, Italy

Supporting Information

ABSTRACT: The ability of Time-Dependent Density Functional Theory (TD-DFT) to provide excited state geometries and reproduce emission energies of organic D-π-A dyes designed for DSSC applications is evaluated. The performance of six functionals (CAM-B3LYP, MPW1K, ωB97X-D, LC-BLYP, LC-ωPBE, and M06-HF) in combination with three basis sets (cc-pVDZ, 6-31+G(d,p), and 6-311+G(2d,p)) has been analyzed. Solvent effects have been taken into account by means of a Polarizable Continuum Model in both LR and SS formalisms. Our LR-PCM/TD-DFT results show that accurate emission energies are obtained only when solvent effects are included in the computation of excited state geometries and when a range separated hybrid functional is used. Vertical emission energies are reproduced with a mean absolute error of at most 0.2 eV. The accuracy is further improved using the SS-PCM formalism.

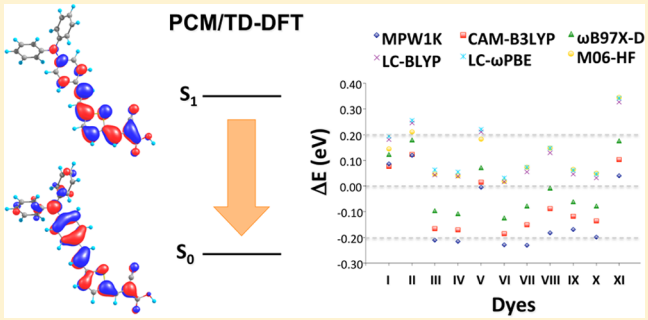

1. INTRODUCTION

Dye-sensitized solar cells (DSSCs) were first introduced in 1991 by O'Regan and Grätzel[1] as a promising alternative to traditional silicon-based photovoltaic cells because of their potentially low economic and environmental costs. DSSCs exploit the capacity of dye sensitizers to generate electron−hole pairs similar to what happens in natural photosynthesis. Indeed, in a DSSC device, the sensitizer, chemically bound to the thin-layer surface of a nanocrystalline semiconductor oxide (generally TiO_2), transfers, upon excitation, an electron to the semiconductor; at the same time, the resulting positive charge (hole) is transferred from the sensitizer to a redox mediator which, through an oxidation−reduction process, carries it to the counter-electrode, thereby closing the circuit and generating an electrical current.[2] It is evident that the dye sensitizer plays a fundamental role for the DSSC working process. In this context, to obtain highly efficient DSSCs, the dye has to fulfill some specific requirements:

i) From the structural point of view, it should contain an anchoring group for adsorption onto the semiconductor surface, in order to provide a stable linkage facilitating electron injection.

ii) The energy of the highest occupied molecular orbital (HOMO) of the dye should be lower than the redox potential of the mediator, while the energy of the lowest unoccupied molecular orbital (LUMO) should be higher than the conduction band edge of the oxide. This ensures to achieve an efficient electron injection and an efficient regeneration of the oxidized state of the dye.

iii) It should be capable of harvesting a wide range of light wavelengths and with high intensity, i.e., the transition governing the photoexcitation should possess a high molar absorption coefficient.

iv) It should be photochemically stable. Its excited state lifetime should be long enough to permit an efficient electron injection before radiative processes or photochemical reactions take place.

The property at point (iv) is extremely important to ensure a good power conversion efficiency (η) of the cell. Thus, the design of new dyes for DSSC could benefit from the evaluation of their photostability in addition to the investigation of their photoexcitation properties.

In the last 20 years a large number of studies have been carried out with the aim of designing and optimizing new DSSC sensitizers (see for example refs 2−4 and references therein). Although traditionally the most efficient sensitizers have been found among metallorganic complexes of ruthenium (η > 11%)[5,6] and, more recently, remarkable results have been obtained by employment of lead-containing perovskites ($\eta \approx$ 15%),[7,8] throughout the years many promising fully organic dyes, mainly

Received: April 16, 2014

   dx.doi.org/10.1021/ct500328t | J. Chem. Theory Comput. XXXX, XXX, XXX−XXX

Scheme 1. Investigated Set of Molecules

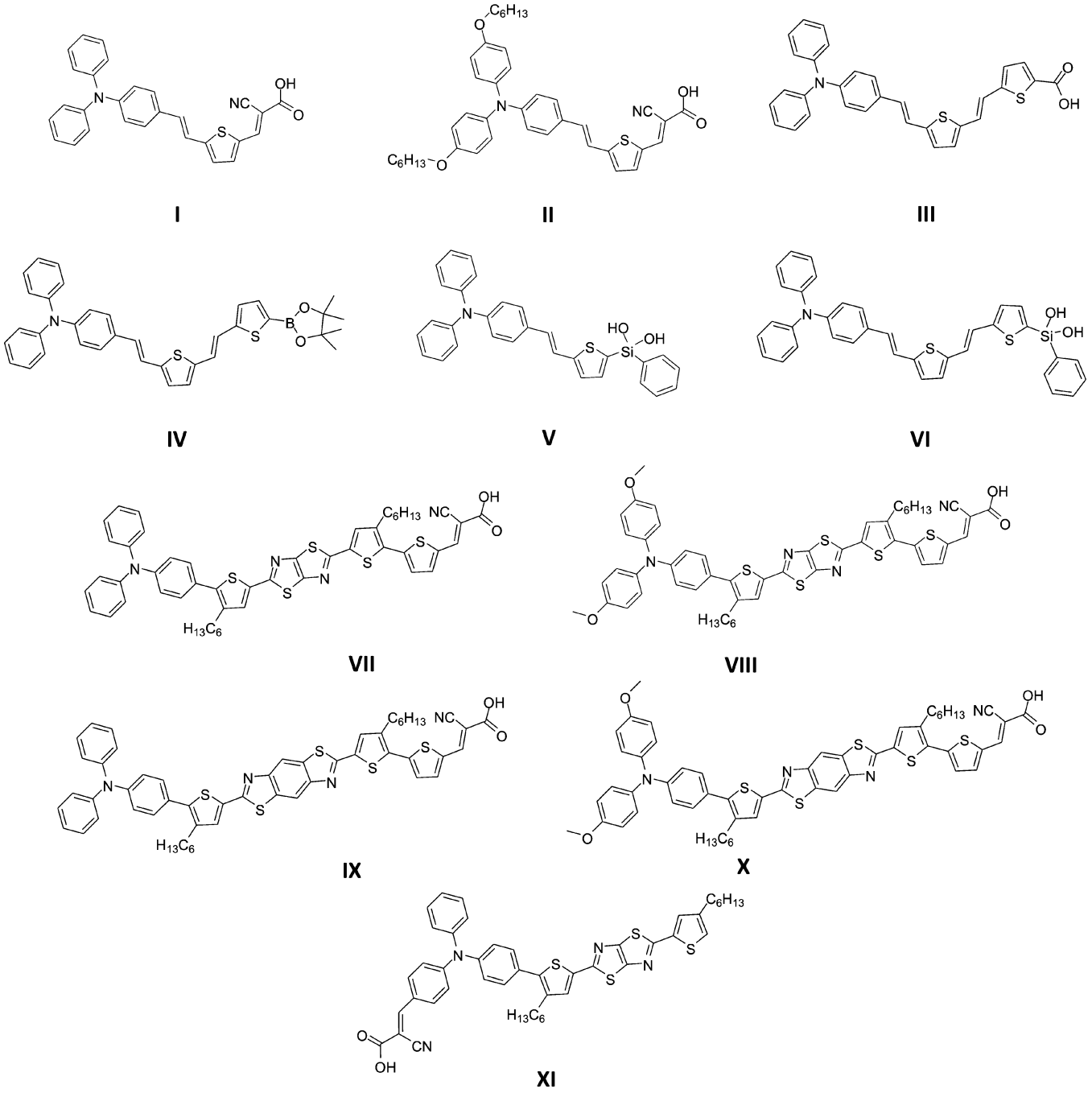

based on a D-π-A structure (i.e., featuring a π conjugated backbone connecting donor and acceptor/anchoring groups), have been proposed and tested, with maximum efficiencies exceeding 10%.[9−15]

Computational studies have played a major role in the design of novel organic sensitizers.[14,16−27] Indeed, using *state-of-the-art* computational methods it has been possible to predict the properties of new materials, e.g., generated by varying their structural components, and identify the most promising ones for which it would be reasonable to plan a synthesis, allowing to accelerate the discovery of new molecules and saving time. Most of the *in silico* studies employed so far focused on the simulations of the absorption properties of isolated dye molecules at the atomic level (either in gas phase or in solution). Density functional theory (DFT) and time-dependent density functional theory (TD-DFT) have been the methods of choice for many of these works, providing very accurate results in terms of reproducing sensitizers optical properties.

In the present study, as a first step toward the exploration of the excited state potential energy surface of the dyes and, therefore, the evaluation of the photostability of D-π-A sensitizers, the excited state geometries and emission maxima of 11 organic dyes used as sensitizers in DSSCs (see molecules **I**−**XI** in Scheme 1) have been computed and compared to the available experimental data using TD-DFT and a polarizable continuum model (PCM)[28] to take into account solvent effects. While compound **I** is the well-known organic dye D5,[17] all the other compounds were prepared for the first time in our group,

dx.doi.org/10.1021/ct500328t | J. Chem. Theory Comput. XXXX, XXX, XXX−XXX

and for most of them the efficiencies of the corresponding photovoltaic devices have already been reported.[13−15] Based on their structural properties, the dyes can be divided into a few groups, namely the following: triarylamine-thiophene derivatives with different conjugation lengths and bearing various anchoring groups (cyanoacrylic acid, carboxylic acid, boronic acid pinacol ester, phenyl silandiol, **I**−**VI**), thiazolothiazole- (**VII**−**VIII**) and benzobisthiazole-containing D-π-A sensitizers (**IX**−**X**), and a single thiazolothiazole-containing sensitizer based on an uncommon π-D-A structure (**XI**).[15]

The performance of six different functionals (CAM-B3LYP,[29] MPW1K,[30,31] ωB97X-D,[32] LC-BLYP,[33−35] LC-ωPBE,[36,37] and M06-HF[38−40]) in combination with cc-pVDZ, 6-31+G(d,p), and 6-311+G(2d,p) basis sets is explored. Emission energies have been computed both in the Linear-Response (LR) and in the State-Specific (SS) formalisms[41] within the PCM/TD-DFT method. Due to the large size of the investigated dyes (10 D-π-A structures plus an unusual π-D-A structure), the widespread use of more conventional excited state methods, such as MR-CI and CASPT2 approaches, is not feasible because of their unfavorable scaling with molecular size.

To the best of our knowledge, this is the first extensive TD-DFT computational study that focuses on the emitting properties of D-π-A dyes. Indeed, there are only a few TD-DFT studies in which the fluorescence emission of a D-π-A dye for DSSC has been computed.[42−44] However, these studies were not intended for benchmarking purposes. Instead, they report emission maxima of a single dye molecule using a single functional or they computed the excited state properties, also using a single functional, on a specific class of model dyes without comparing them to any available experimental data. Besides, the solvation effects were introduced only for the calculation of the vertical emission energies and not at the optimization stage, while in the present paper the role of the solvation in affecting the excited state geometries has been explored. It is also worth noting that this is the first computational investigation of excited state geometry and emission properties of one of the most representative organic dyes for DSSC, i.e., the D5 dye (molecule **I** in Scheme 1).

The results showed that the use of the PCM/TD-DFT method in computing the low-lying singlet excited state of the 11 dyes allowed obtaining emission data that compare well with the experimental values. Indeed, the mean absolute error (MAE) is, in the best cases, 0.10 eV.

The possibility to use TD-DFT functionals to obtain excited state geometries and reproduce emission maxima with a satisfying level of accuracy opens the way to the study of the excited state potential energy surface of these dyes and the evaluation of their photostability, in turn giving the possibility to design improved compounds, in terms of excited state stability, through substitutions and/or insertion of different molecular units.

2. COMPUTATIONAL DETAILS

All QM calculations have been performed using the Gaussian 09, Revision C.01 suite of programs.[45]

First singlet excited-state (S_1) geometry optimizations on the 11 dyes in Scheme 1 were performed by TD-DFT calculations, including solvent effects, at the LR-PCM/TD-B3LYP/6-31G(d) and PCM/TD-CAM-B3LYP/6-31G(d) levels. [For molecule **I** PCM/TD-CAM-B3LYP optimizations have also been performed using cc-pVDZ, 6-31+G(d,p) and 6-311+G(2d,p) basis sets to test the basis set dependence of the computed S1 geometry. Results are gathered in Table S12.]

We have modeled the same solvents used in the experiments (see the list of solvents given in Table 1). S_1 geometries were obtained in an equilibrium solvation regime. For comparison and to test the effect of the solvent on the geometry optimization, excited state geometries have also been obtained *in vacuo* at the TD-CAM-B3LYP/6-31G(d) level.

Table 1. Solvents and Experimental Values Used As Reference in This Study[a]

molecule	solvent	λ_{max} (nm)	E_{emi} (eV)
I	ethanol	621[b]	2.00
II	ethanol	656[c]	1.89
III	tetrahydrofuran	557[d]	2.23
IV	tetrahydrofuran	535[d]	2.32
V	methanol	470[e]	2.64
VI	methanol	528[e]	2.35
VII	tetrahydrofuran	581[f]	2.13
VIII	tetrahydrofuran	605[f]	2.05
IX	tetrahydrofuran	537[f]	2.31
X	tetrahydrofuran	534[f]	2.32
XI	methanol	563[g]	2.20

[a]Molecules are shown in Scheme 1. [b]Data taken from ref 16. [c]Data taken from ref 46. [d]This work. [e]Data taken from ref 13. [f]Data taken from ref 14. [g]Data taken from ref 15.

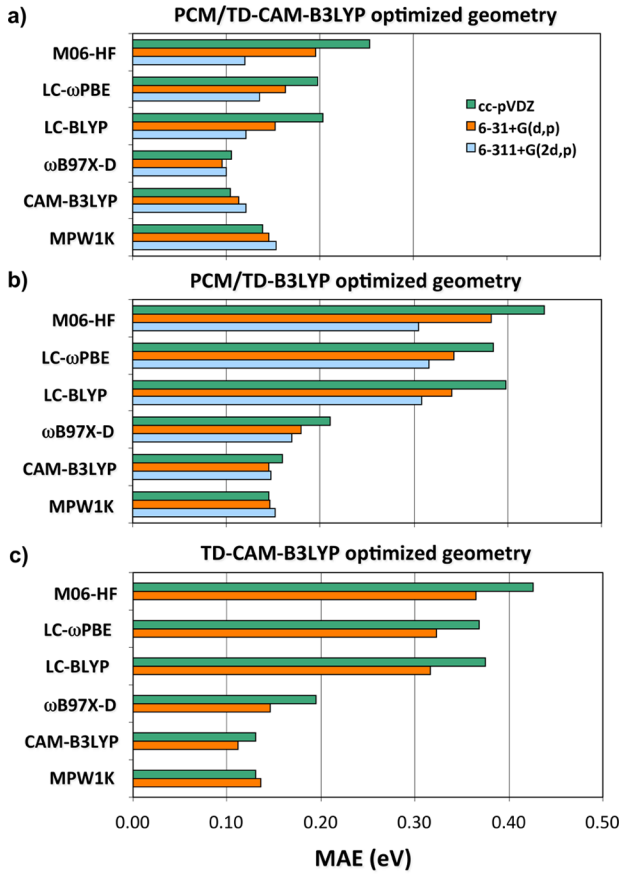

Figure 1. MAE obtained for the LR-PCM/TD-DFT computed vertical emission energies of the 11 dyes in Scheme 1. The experimental values used as references are listed in Table 1. The 11 molecules are optimized at the a) PCM/TD-CAM-B3LYP/6-31G(d), b) PCM/TD-B3LYP/6-31G(d), and c) TD-CAM-B3LYP/6-31G(d) levels.

dx.doi.org/10.1021/ct500328t | J. Chem. Theory Comput. XXXX, XXX, XXX−XXX

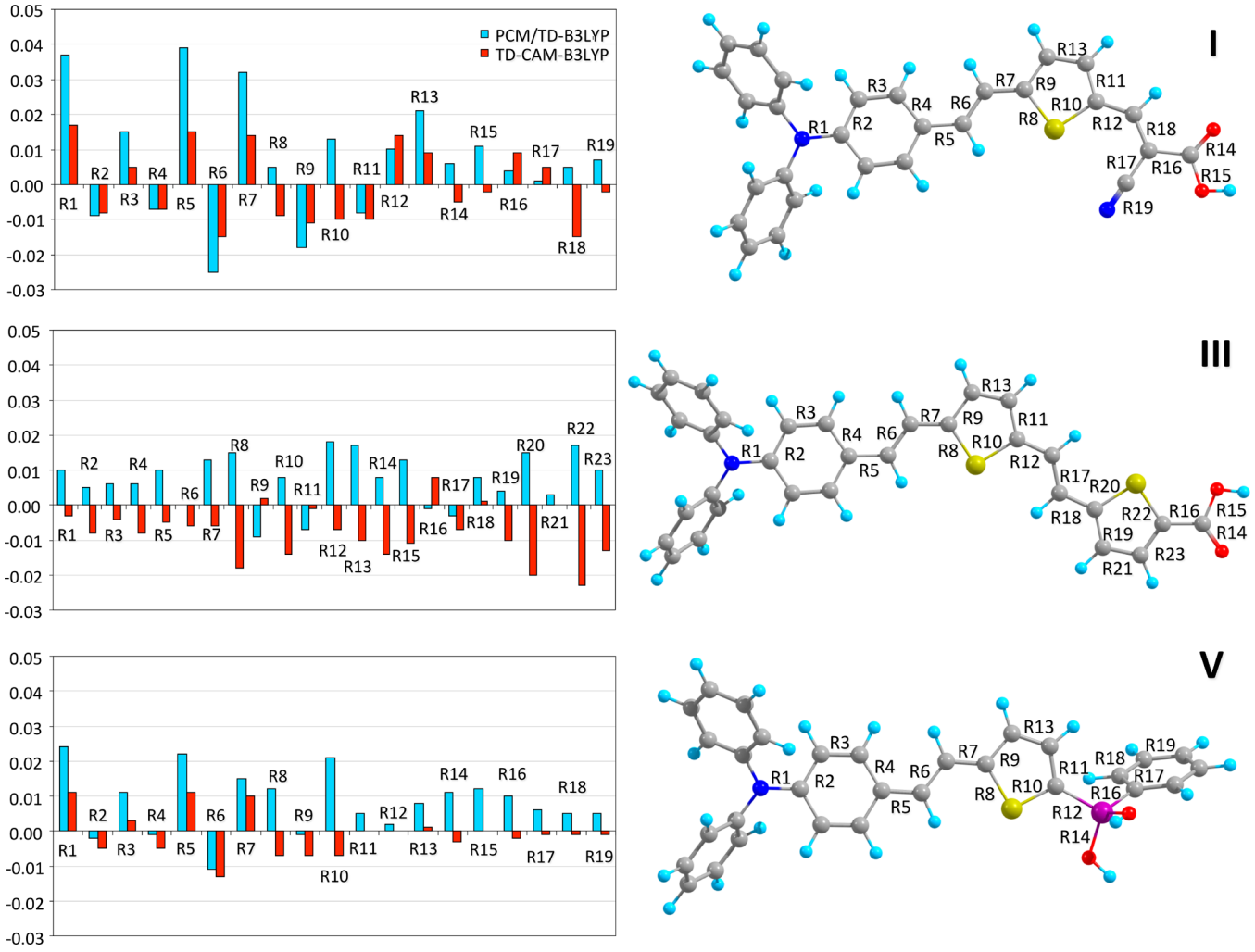

Figure 2. Bond length variations in molecules **I**, **III**, and **V** optimized at the PCM/TD-B3LYP/6-31G(d) and TD-CAM-B3LYP/6-31G(d) levels compared to the PCM/TD-CAM-B3LYP/6-31G(d) level.

The emission maxima have been computed on all the optimized geometries employing six different exchange-correlation (xc) functionals including long-range corrected and range separated hybrid functionals (LC-ωPBE, LC-BLYP, CAM-B3LYP, ωB97X-D), a global hybrid meta GGA functional (M06-HF), and a hybrid GGA functional (MPW1K) in combinations with the Dunning's cc-pVDZ, the Pople's 6-31+G(d,p) and 6-311+G(2d,p) basis sets. [For molecules **I** and **VII** additional calculations have been performed to check the effect of different isomeric structures and of the conformational flexibility of substituents on the computed vertical emission energies. For further details see Tables S6−S10 and Figures S2 and S3.] The tested functionals have been selected on the basis of previous benchmarks[47−51] where they have been shown to be promising for the description of charge transfer excitations. Indeed the emission process of the studied dyes displays a charge transfer character (see the discussion below).

Bulk solvent effects have been taken into account using the LR implementation of PCM/TD-DFT methods for geometry optimization and vertical emission energies. The new state specific (SS) implementation[27,41,52] of TD-DFT has been applied to perform corrections on the vertical emission energies at the PCM/TD-CAM-B3LYP/6-31+G(d,p), PCM/TD-CAM-B3LYP/6-311+G(2d,p), PCM/TD-ωB97X-D/6-31+G(d,p), and PCM/TD-ωB97X-D/6-311+G(2d,p) on PCM/TD-CAM-B3LYP/6-31G(d) optimized geometries.

Additional calculations aimed to benchmark the different TD-DFT approaches with respect to high level multireference perturbation theory (CASPT2) and coupled cluster methods have been performed in the gas-phase and for the smallest dye (molecule **I**). The results are summarized in Table S11.

3. RESULTS

The present benchmarking study aims to evaluate the performance of six selected DFT functionals (CAM-B3LYP, MPW1K, ωB97X-D, LC-BLYP, LC-ωPBE, and M06-HF) in the calculation of the vertical emission energies of D-π-A (plus an unusual π-D-A structure) dyes for DSSC. The effect of these functionals is analyzed in combinations with 3 basis sets (cc-pVDZ, 6-31+G(d,p), and 6-311+G(2d,p)) and at two different geometry optimization levels (PCM/TD-CAM-B3LYP/6-31G(d) and PCM/TD-B3LYP/6-31G(d)). Additionally, to test the effect of the solvent on geometry optimization, the vertical emission energies have also been computed using the six functionals in combination with cc-pVDZ and 6-31+G(d,p) basis sets on the excited-state geometries obtained *in vacuo* at the TD-CAM-B3LYP/6-31G(d) level. Initially, the LR formalism of the PCM method is used to include solvent effects. The complete set of vertical emission energies

dx.doi.org/10.1021/ct500328t | J. Chem. Theory Comput. XXXX, XXX, XXX−XXX

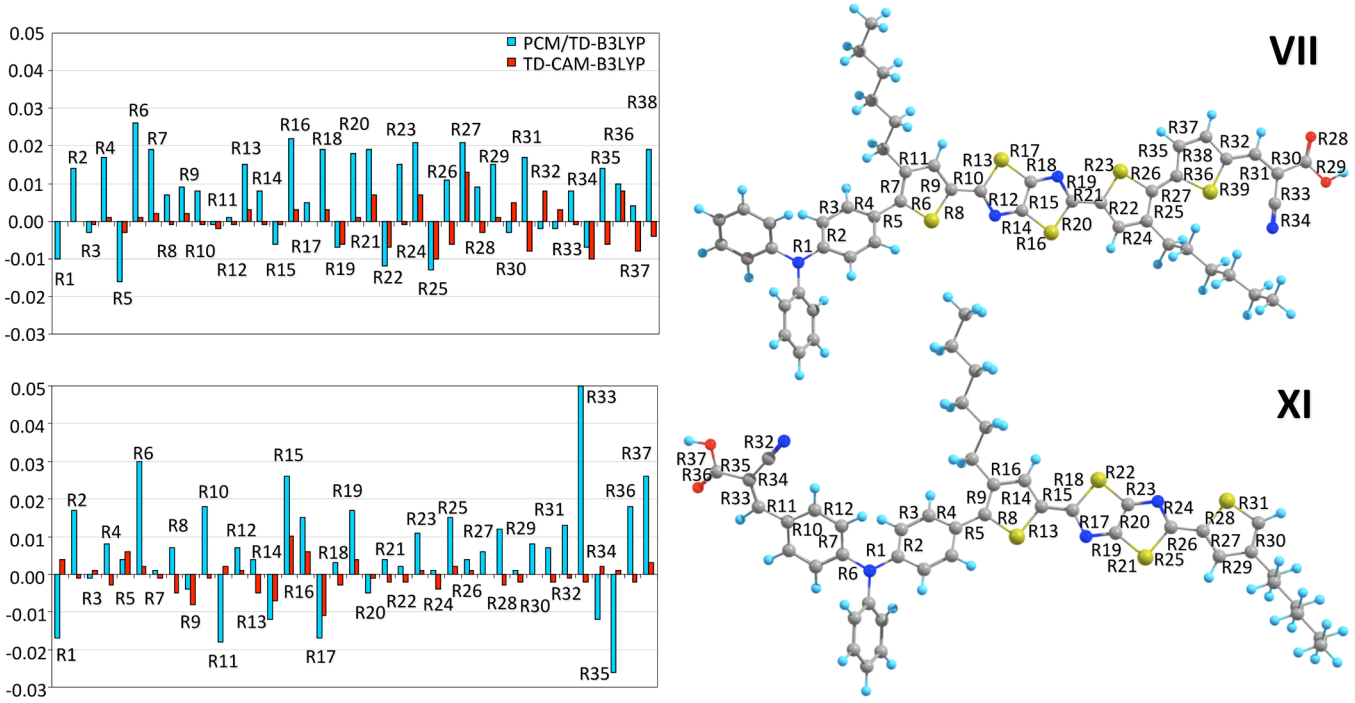

Figure 3. Bond length variations in molecules **VII** and **XI** optimized at the PCM/TD-B3LYP/6-31G(d) and TD-CAM-B3LYP/6-31G(d) levels compared to the PCM/TD-CAM-B3LYP/6-31G(d) level.

(*E*, eV) and associated oscillator strengths (*f*) for dyes **I**–**XI** is shown in Table S1, S2, and S3.

The relative performance of the six selected functionals can be appreciated from Figure 1, which shows the mean absolute error (MAE) obtained in the computation of the $S_1 \rightarrow S_0$ emission maxima of the 11 sensitizers reported in Scheme 1.

Focusing on the PCM/TD-CAM-B3LYP optimized structures (Figure 1a), the MAE analysis clearly shows that among the chosen DFT functionals, three of them (CAM-B3LYP, MPW1K, ωB97X-D) behave very well presenting MAE values of at most 0.15 eV. The influence of the chosen basis set in combinations with CAM-B3LYP, MPW1K, and ωB97X-D functionals is not very relevant. The other functionals (LC-BLYP, LC-ωPBE, and M06-HF), despite providing poorer results, have MAE values that are at most equal to 0.20 eV, with the only exception of the M06-HF/cc-pVDZ level. The effect of the basis set is much more evident using the LC-BLYP, LC-ωPBE, and M06-HF functionals. Indeed, the use of the 6-311+G(2d,p) basis set significantly lowers the MAE.

The impact of the geometry optimization level on the vertical emission energies has been taken into account optimizing the sensitizers at the less expensive PCM/TD-B3LYP level (Figure 1b). Although it is not possible to completely decouple the accuracy in the calculation of the excitation energies and of the excited state geometries, it is evident that the agreement with the experimental values is worse for the vertical emission energies computed on the PCM/TD-B3LYP geometries. Furthermore, the importance of including solvent effects at the optimization level is clear considering the results in Figure 1c. Indeed, similarly to the results in Figure 1b, the minimization *in vacuo* at the CAM-B3LYP/6-31G(d) level increases the discrepancy with respect to the experimental data moving the MAE values toward 0.4 eV.

All the dyes assume a largely planar structure along the conjugated system; the only substantial deviation from coplanarity was found at the thiophene-phenyl junction of molecules **VII**, **VIII**, **IX**, **X**, and **XI**, with dihedral angles of at most 46° at the PCM/TD-CAM-B3LYP/6-31G(d) level, due to steric reasons. The most relevant changes in geometries are related to bond lengths, and their variations are shown in Figures 2 and 3. For the sake of clarity, we limit our discussion to molecules **I**, **III**, **V**, **VII**, and **XI** as representative members of the different groups of dyes considered in this study.

Bond length changes are within 0.02 Å considering the effect of introducing the PCM environment in the calculation of the geometries (PCM/TD-CAM-B3LYP vs TD-CAM-B3LYP optimized geometries), while the same changes increase toward 0.05 Å using the B3LYP functional (PCM/TD-CAM-B3LYP vs PCM/TD-B3LYP optimized geometries).

Figure 4 gives a quantification of the effect due to the introduction of the solvent (TD-CAM-B3LYP vs PCM/TD-CAM-B3LYP, see the ordinate) in comparison to the effect due to the choice of the functional (PCM/TD-B3LYP vs PCM/TD-CAM-B3LYP, see the abscissa) in computing vertical emission energies. Looking at the energy differences (eV) between errors in computing vertical emission energies, taking the PCM/TD-CAM-B3LYP results as reference values, it is evident that the most significant deviations from the zero are along the abscissa (i.e., considering the effect of the functional), especially for molecules **I** and **II** (0.21 and 0.24 eV, respectively). The only important deviation on the ordinate (i.e., considering the effect of the solvent) is obtained for molecule **XI** (0.19 eV). Thus, we could argue that for the studied dyes the effect of the solvent is less critical than the use of CAM-B3LYP instead of B3LYP functional to optimize the excited state D-π-A structures. This parallels the larger variation for the PCM/TD-B3LYP optimized geometries (see blue bars in Figures 2 and 3) compared to the smaller variation obtained for the geometries optimized *in vacuo* at the TD-CAM-B3LYP level (see red bars in Figures 2 and 3).

dx.doi.org/10.1021/ct500328t | J. Chem. Theory Comput. XXXX, XXX, XXX–XXX

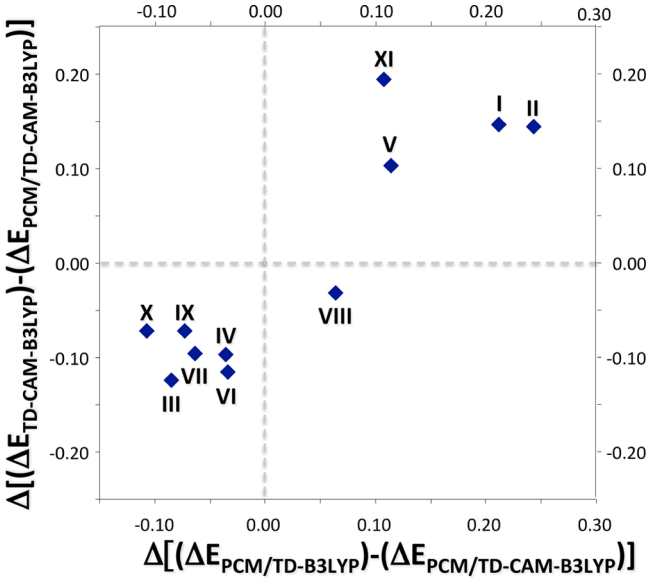

Figure 4. Energy differences (eV) between errors in computing vertical emission energies at LR-PCM/TD-B3LYP/6-31+G(d,p) and TD-CAM-B3LYP/6-31+G(d,p) levels compared to those computed at LR-PCM/TD-CAM-B3LYP/6-31+G(d,p) (taken as reference value) for the set of molecules optimized at the PCM/TD-CAM-B3LYP/6-31G(d) level.

By looking at the histograms in Figure 5, it is quite clear that LC-BLYP, LC-ωPBE, and M06-HF functionals provide overestimated emission energies, while CAM-B3LYP, MPW1K, and ωB97X-D provide emission energies within 0.2 eV of the experimental values, with few exceptions. Remarkably, the three functionals that tend to overestimate the computed emission energies are those with particularly large percentages of Hartree−Fock exchange (HFX).

To better understand which molecules among the 11 studied dyes are possibly more problematic to treat at the PCM/TD-DFT level, in Figure 6 we plotted the energy differences between LR-PCM/TD-DFT vertical emission energies (for the set of molecules optimized at the PCM/TD-CAM-B3LYP/6-31G(d) level) and experimental fluorescence energies. The graph shows that all the dyes are well described by all the functionals (with a ΔE ca. $\pm$ 0.2 eV) with the only exception of dye **II** when LC-BLYP and LC-ωPBE (with a $\Delta E \approx 0.25$ eV) functionals are used and dye **XI** that diverges significantly (with a ΔE > 0.3 eV) using LC-BLYP, LC-ωPBE, and M06-HF functionals. On the other hand, dye **XI** is more properly described as a π-D-A rather than a D-π-A structure, as can be seen from the fact that its donor and acceptor groups are directly linked to each other, with the conjugate unit stemming from the triphenylamine moiety (Scheme 1).[15]

The computed electronic transitions of the 11 molecules reveal that the emission process is mainly due to a LUMO → HOMO transition in the case of molecules **I**−**VIII** and **XI**, accounting for ≥90% of the total for molecules **I**-**VI**, and almost 70, 60, 80% for dyes **VII**, **VIII**, and **XI**, respectively. A LUMO → HOMO−1 transition is instead governing the emission process in molecules **IX** and **X**. These transitions are all intense with oscillator strengths of up to 2.60 (molecule **VIII**). Their charge transfer (CT) character can be inferred looking at the shape of the frontier molecular orbitals (FMOs) involved. In Figure 7 the HOMOs and LUMOs for molecules **I, III, V, VII,** and **XI** (the same set of molecules chosen for the geometry analysis) are

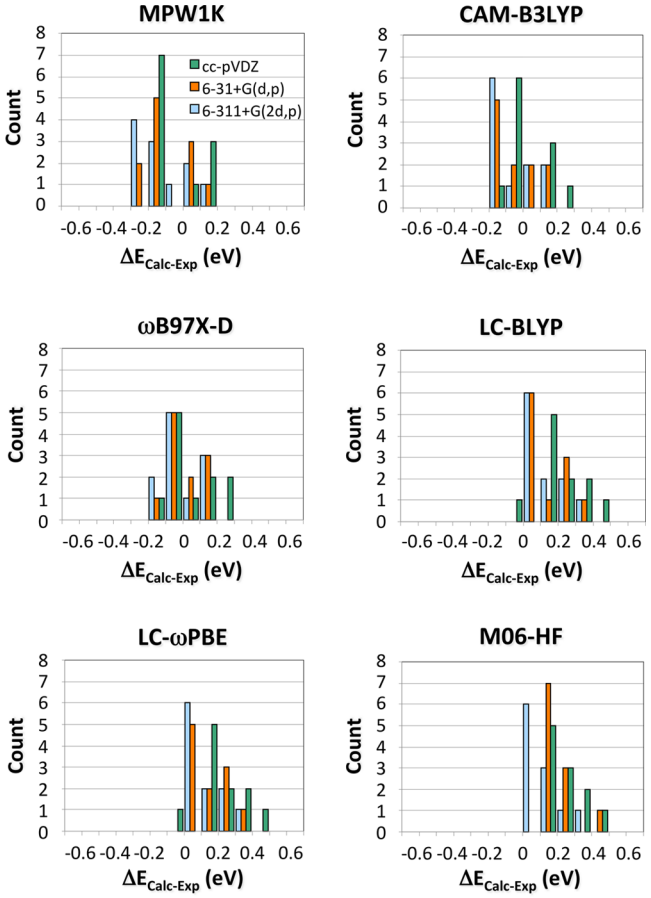

Figure 5. Histograms of the errors obtained when comparing the LR-PCM/TD-DFT vertical emission energies to the experimental emission energies for the set of molecules optimized at the PCM/TD-CAM-B3LYP/6-31G(d) level.

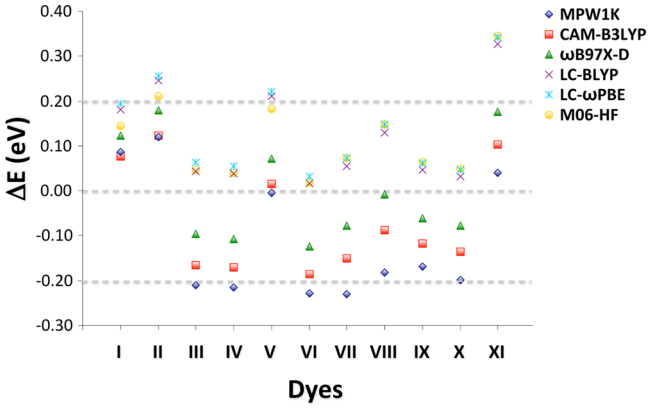

Figure 6. Energy differences (eV) between LR-PCM/TD-DFT/6-311+G(2d,p) vertical emission energies and experimental emission energies for the set of molecules optimized at the PCM/TD-CAM-B3LYP/6-31G(d) level.

presented. Plots of the HOMO−1, HOMO, LUMO, and LUMO+1 orbitals for all the computed molecules and further details on their emission transitions are shown in Table S4 of the Supporting Information.

In molecules **I, III,** and **VII**, LUMOs are mainly located on the acceptor moieties, while HOMOs are mainly localized on the conjugated scaffold (D-π portion) of the molecules.

dx.doi.org/10.1021/ct500328t | J. Chem. Theory Comput. XXXX, XXX, XXX−XXX

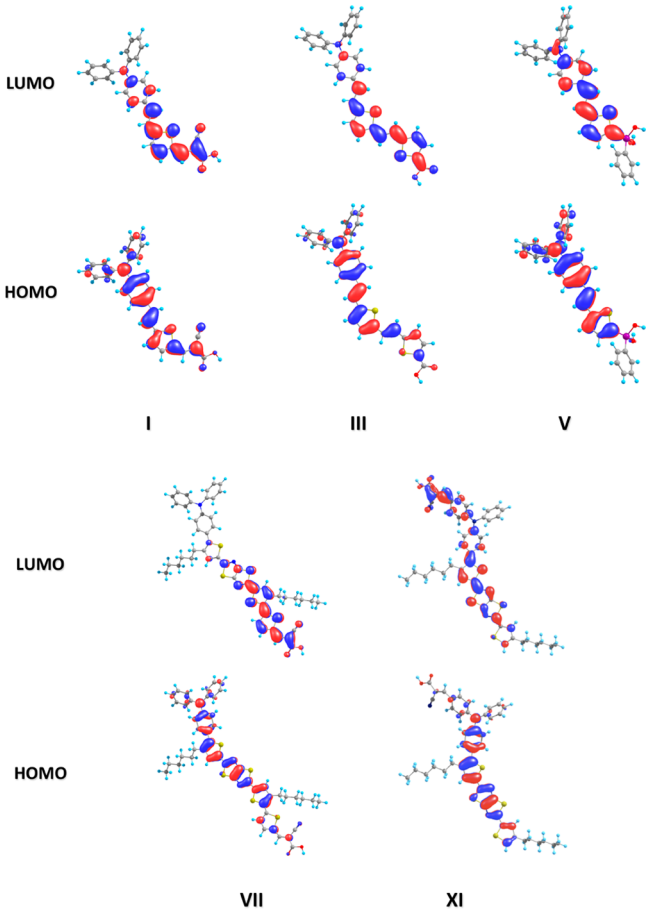

Figure 7. LUMOs and HOMOs for molecule **I**, **III**, **V**, **VII**, and **XI** obtained at the PCM-CAM-B3LYP/6-31G(d) level.

This distribution of the FMOs supports the charge transfer nature of the emission process. In the case of molecule **V**, the acceptor moiety is less involved at the LUMO level thus limiting the CT to the D-π portion of the molecule. Despite its unusual π-D-A structure, molecule **XI** shows a similar shape of the FMOs with the LUMO located on the cyanoacrylic group, with a smaller contribution of the triphenylamine moiety, and the HOMO mainly localized on the conjugate system centered on the thiazolothiazole bridge, thus supporting, even in this case, the charge transfer character of the emission transition.

In the last part of this study, the impact of using a state specific (SS) model for the inclusion of solvent effects in TD-DFT computations of emission energies of the 11 dyes is assessed. Within the SS model it is possible to take into account the excited state density of the state of interest allowing for a complete description of the mutual solvent−solute polarization. The results of SS- and LR-PCM/TD-DFT methods are compared for the considered emission processes in Figure 8. We computed the emission maxima of the 11 dyes at the SS-PCM/TD-CAM-B3LYP/6-31+G(d,p), SS-PCM/TD-CAM-B3LYP/6-311+G-(2d,p), SS-PCM/TD-ωB97X-D/6-31+G(d,p), and SS-PCM/TD-ωB97X-D/6-311+G(2d,p) levels on PCM/TD-CAM-B3LYP/6-31G(d) optimized geometries and compared the results with those provided by LR-PCM calculations. We limit our analysis to SS-PCM/TD-ωB97X-D and SS-PCM/TD-CAM-B3LYP levels because they exhibited the lowest MAE values. The SS-PCM/TD-DFT vertical emission energies (E, eV) and associated oscillator strengths (f) for the investigated $S_1 \rightarrow S_0$ transitions are reported in Table S5 of the Supporting Information.

The overall effect is that the SS-PCM values improve the computed vertical emission energies at both the CAM-B3LYP and ωB97X-D levels of theory. Indeed, the error is now falling within ±0.15 eV for all computed dyes with the only exception of molecule **XI**, at the ωB97X-D level. Although dye **XI** together with dyes **I** and **VIII** are negatively affected by the use of the SS-PCM treatment, the shifts involved are limited (<2%), and the

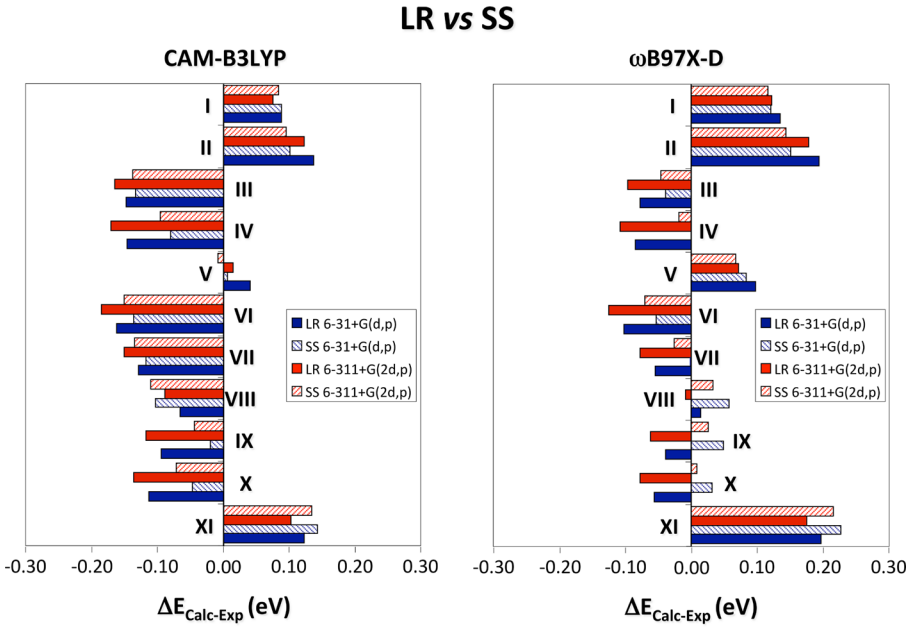

Figure 8. Histograms of the errors (in eV) obtained when comparing the LR-PCM/TD-DFT and SS-PCM/TD-DFT results to the experimental emission energies. Vertical emission energies are computed with the SS-PCM and LR-PCM methods using the CAM-B3LYP and ωB97X-D functionals in combination with the 6-311+G(2d,p) and 6-31+G(d,p) basis sets.

dx.doi.org/10.1021/ct500328t | J. Chem. Theory Comput. XXXX, XXX, XXX−XXX

LR-PCM/TD-DFT errors in computing emission energies, except for molecule **XI**, are very small (within 0.10 eV).

Finally, as shown in Figure S1 of the Supporting Information, the computed shifts (SS-PCM vs LR-PCM) for the vertical emission energies are up to 0.07 eV (for CAM-B3LYP) and 0.09 (for ωB97X-D) toward the experimental values, using both the 6-31+G(d,p) and 6-311+G(2d,p) basis set.

4. CONCLUSIONS

In summary, we showed that the use of the tested functionals (LC-ωPBE, LC-BLYP, CAM-B3LYP, ωB97X-D, M06-HF, MPW1K) within the PCM/TD-DFT method allows attaining accurate emission energies of the lowest-lying excited states of D-π-A dyes. In particular, ωB97X-D and CAM-B3LYP demonstrated better performance than the other functionals, giving the lowest MAE values. The inclusion of solvent effects at the optimization stage is crucial to obtain results that are consistent with experimental values (∼0.2 eV). The use of a SS-PCM model further reduces the discrepancy with experiments (within 0.15 eV).

We believe that our benchmarking study will be important to further research in the field of DSSCs, in particular for the evaluation of the photostability of D-π-A sensitizers. A better assessment of such parameter will allow the design of more robust organic dyes, in turn resulting in more reliable and durable photovoltaic devices.

■ ASSOCIATED CONTENT

Supporting Information

Tables with vertical emission energies (E, eV) and associated oscillator strengths (f) computed at LR- and SS-PCM/TD-DFT levels; FMOs plots; additional results. This material is available free of charge via the Internet at http://pubs.acs.org.

■ AUTHOR INFORMATION

Corresponding Author

*E-mail: adalgisa.sinicropi@unisi.it.

Notes

The authors declare no competing financial interest.

■ ACKNOWLEDGMENTS

The authors are grateful to Regione Toscana within the POR-FSE 2007-2013 program ("FOTOSENSORG" project). We acknowledge the CINECA Awards N. HP10CJ65S2 and HP10CXBWGO and C.R.E.A (Centro Ricerche Energia e Ambiente, Colle Val D'Elsa, Siena, Italy) for the availability of high performance computing resources and support.

■ REFERENCES

(1) O'Regan, B.; Grätzel, M. *Nature* **1991**, *353*, 737−740.
(2) Hagfeldt, A.; Boschloo, G.; Sun, L.; Kloo, L.; Pettersson, H. *Chem. Rev.* **2010**, *110*, 6595−6663.
(3) Gong, J.; Liang, J.; Sumathy, K. *Renewable Sustainable Energy Rev.* **2012**, *16*, 5848−5860.
(4) Zhang, S.; Yang, X.; Numata, Y.; Han, L. *Energy Environ. Sci.* **2013**, *6*, 1443−1464.
(5) Nazeeruddin, M. K.; Kay, A.; Rodicio, L.; Humphry-Baker, R.; Müller, E.; Liska, P.; Vlachopoulos, N.; Grätzel, M. *J. Am. Chem. Soc.* **1993**, *115*, 6382−6390.
(6) Han, L.; Islam, A.; Chen, H.; Malapaka, C.; Chiranjeevi, B.; Zhang, S.; Yang, X.; Yanagida, M. *Energy Environ. Sci.* **2012**, *5*, 6057−6060.
(7) Snaith, H. J. *J. Phys. Chem. Lett.* **2013**, *4*, 3623−3630.
(8) Kazim, S.; Nazeeruddin, M. K.; Grätzel, M.; Ahmad, S. *Angew. Chem., Int. Ed.* **2014**, *53*, 2812−2824.
(9) Ooyama, Y.; Harima, Y. *ChemPhysChem* **2012**, *13*, 4032−4080.
(10) Kanaparthi, R. K.; Kandhadi, J.; Giribabu, L. *Tetrahedron* **2012**, *68*, 8383−8393.
(11) Wu, Y.; Zhu, W. *Chem. Soc. Rev.* **2013**, *42*, 2039−2058.
(12) Kim, B.-G.; Chung, K.; Kim, J. *Chem.—Eur. J.* **2013**, *19*, 5220−5230.
(13) Barozzino Consiglio, G.; Pedna, F.; Fornaciari, G.; Fabrizi de Biani, F.; Marotta, G.; Salvatori, P.; Basosi, R.; De Angelis, F.; Mordini, A.; Parisi, M. L.; Peruzzini, M.; Reginato, G.; Taddei, M.; Zani, L. *J. Organomet. Chem.* **2013**, *723*, 198−206.
(14) Dessì, A.; Barozzino Consiglio, G.; Calamante, M.; Reginato, G.; Mordini, A.; Peruzzini, M.; Taddei, M.; Sinicropi, A.; Parisi, M. L.; Fabrizi de Biani, F.; Basosi, R.; Mori, R.; Spatola, M.; Bruzzi, M.; Zani, L. *Eur. J. Org. Chem.* **2013**, *2013*, 1916−1928.
(15) Zani, L.; Reginato, G.; Mordini, A.; Calamante, M.; Peruzzini, M.; Taddei, M.; Sinicropi, A.; Parisi, M. L.; Fabrizi de Biani, F.; Basosi, R.; Cavallaro, A.; Bruzzi, M. *Tetrahedron Lett.* **2013**, *54*, 3944−3948.
(16) Hagberg, D. P.; Yum, J.-H.; Lee, H.; De Angelis, F.; Marinado, T.; Karlsson, K. M.; Humphry-Baker, R.; Sun, L.; Hagfeldt, A.; Grätzel, M.; Nazeeruddin, M. K. *J. Am. Chem. Soc.* **2008**, *130*, 6259−6266.
(17) Hagberg, D. P.; Edvinsson, T.; Marinado, T.; Boschloo, G.; Hagfeldt, A.; Sun, L. *Chem. Commun.* **2006**, 2245−2247.
(18) Preat, J.; Michaux, C.; Jacquemin, D.; Perpète, E. A. *J. Phys. Chem. C* **2009**, *113*, 16821−16833.
(19) Meng, S.; Kaxiras, E.; Nazeeruddin, M. K.; Grätzel, M. *J. Phys. Chem. C* **2011**, *115*, 9276−9282.
(20) Le Bahers, T.; Labat, F.; Pauporté, T.; Lainé, P. P.; Ciofini, I. *J. Am. Chem. Soc.* **2011**, *133*, 8005−8013.
(21) Labat, F.; Le Bahers, T.; Ciofini, I.; Adamo, C. *Acc. Chem. Res.* **2011**, *45*, 1268−1277.
(22) Pastore, M.; Mosconi, E.; De Angelis, F.; Grätzel, M. *J. Phys. Chem. C* **2010**, *114*, 7205−7212.
(23) Marotta, G.; Reddy, M. A.; Singh, S. P.; Islam, A.; Han, L. Y.; De Angelis, F.; Pastore, M. *ACS Appl. Mater. Interfaces* **2013**, *5*, 9635−9647.
(24) Longhi, E.; Bossi, A.; Di Carlo, G.; Maiorana, S.; De Angelis, F.; Salvatori, P.; Petrozza, A.; Binda, M.; Roiati, V.; Mussini, P. R. *Eur. J. Org. Chem.* **2013**, 84−94.
(25) Li, H. X.; Chen, M. D. *J. Mol. Model.* **2013**, *19*, 5317−5325.
(26) Wang, J.; Gong, S.; Wen, S. Z.; Yan, L. K.; Su, Z. M. *J. Phys. Chem. C* **2013**, *117*, 2245−2251.
(27) De Mitri, N.; Monti, S.; Prampolini, G.; Barone, V. *J. Chem. Theory Comput.* **2013**, *9*, 4507−4516.
(28) Tomasi, J.; Mennucci, B.; Cammi, R. *Chem. Rev.* **2005**, *105*, 2999−3094.
(29) Yanai, T.; Tew, D. P.; Handy, N. C. *Chem. Phys. Lett.* **2004**, *393*, 51−56.
(30) Lynch, B. J.; Fast, P. L.; Harris, M.; Truhlar, D. G. *J. Phys. Chem. A* **2000**, *104*, 4811−4815.
(31) Zhao, J.; Lynch, B. J.; Truhlar, D. G. *J. Phys. Chem. A* **2004**, *108*, 2715−2719.
(32) Chai, J. D.; Head-Gordon, M. *Phys. Chem. Chem. Phys.* **2008**, *10*, 6615−6620.
(33) Ikura, H.; Tsuneda, T.; Yanai, T.; Hirao, K. *J. Chem. Phys.* **2001**, *115*, 3540−3544.
(34) Slater, J. C. *Quantum Theory of Molecular and Solids*; McGraw-Hill: New York, 1974; Vol. *4*.
(35) Lee, C.; Yang, W.; Parr, R. G. *Phys. Rev. B* **1988**, *37*, 785−789.
(36) Vydrov, O. A.; Scuseria, G. E. *J. Chem. Phys.* **2006**, *125*, 234109.
(37) Vydrov, O. A.; Heyd, J.; Krukau, V.; Scuseria, G. E. *J. Chem. Phys.* **2006**, *125*, 074106.
(38) Zhao, Y.; Truhlar, D. G. *J. Phys. Chem. A* **2006**, *110*, 5121−5129.
(39) Zhao, J.; Truhlar, D. G. *Theor. Chem. Acc.* **2008**, *120*, 215−241.
(40) Zhao, J.; Truhlar, D. G. *J. Chem. Phys.* **2006**, *125*, 194101.
(41) Improta, R. In *Computational Strategies for Spectroscopy: From Small Molecules to Nano Systems*; Barone, V., Ed.; John Wiley & Sons, Inc.: 2012; pp 39.

(42) Fakis, M.; Hrobárik, P.; Stathatos, E.; Giannetas, V.; Persephonis, P. *Dyes Pigm.* **2013**, *96*, 304−312.
(43) Shi, H.; Dai, J.; Shi, L.; Xu, L.; Zhou, Z.; Zhang, Y.; Zhou, W.; Dong, C. *Spectrochim. Acta, Part A* **2012**, *93*, 19−25.
(44) Fitri, A.; Benjelloun, A. T.; Benzakour, M.; Mcharfi, M.; Hamidi, M.; Bouachrine, M. *Spectrochim. Acta, Part A* **2014**, *124*, 646−654.
(45) Frisch, M. J.; Trucks, G. W.; Schlegel, H. B.; Scuseria, G. E.; Robb, M. A.; Cheeseman, J. R.; Scalmani, G.; Barone, V.; Mennucci, B.; Petersson, G. A.; Nakatsuji, H.; Caricato, M.; Li, X.; Hratchian, H. P.; Izmaylov, A. F.; Bloino, J.; Zheng, G.; Sonnenberg, J. L.; Hada, M.; Ehara, M.; Toyota, K.; Fukuda, R.; Hasegawa, J.; Ishida, M.; Nakajima, T.; Honda, Y.; Kitao, O.; Nakai, H.; Vreven, T.; Montgomery, J. A., Jr.; Peralta, J. E.; Ogliaro, F.; Bearpark, M.; Heyd, J. J.; Brothers, E.; Kudin, K. N.; Staroverov, V. N.; Keith, T.; Kobayashi, R.; Normand, J.; Raghavachari, K.; Rendell, A.; Burant, J. C.; Iyengar, S. S.; Tomasi, J.; Cossi, M.; Rega, N.; Millam, J. M.; Klene, M.; Knox, J. E.; Cross, J. B.; Bakken, V.; Adamo, C.; Jaramillo, J.; Gomperts, R.; Stratmann, R. E.; Yazyev, O.; Austin, A. J.; Cammi, R.; Pomelli, C.; Ochterski, J. W.; Martin, R. L.; Morokuma, K.; Zakrzewski, V. G.; Voth, G. A.; Salvador, P.; Dannenberg, J. J.; Dapprich, S.; Daniels, A. D.; Farkas, O.; Foresman, J. B.; Ortiz, J. V.; Cioslowski, J.; Fox, D. J. *Gaussian 09*, Revision C.01; Gaussian, Inc.: Wallingford, CT, 2010.
(46) Franchi, D.; Calamante, M.; Reginato, G.; Zani, L.; Peruzzini, M.; Taddei, M.; Fabrizi de Biani, F.; Basosi, R.; Sinicropi, A.; Colonna, D.; Di Carlo, A.; Mordini, A. *Tetrahedron* **2014**, *70*, 6285−6295.
(47) Jacquemin, D.; Wathelet, V.; Perpète, E. A.; Adamo, C. *J. Chem. Theory Comput.* **2009**, *5*, 2420−2435.
(48) Bousquet, D.; Fukuda, R.; Maitarad, P.; Jacquemin, D.; Ciofini, I.; Adamo, C.; Ehara, M. *J. Chem. Theory Comput.* **2013**, *9*, 2368−2379.
(49) Peach, M. J. G.; Benfield, P.; Helgaker, T.; Tozer, D. J. *J. Chem. Phys.* **2008**, *128*, 044118.
(50) Charaf-Eddin, A.; Planchat, A.; Mennucci, B.; Adamo, C.; Jacquemin, D. *J. Chem. Theory Comput.* **2013**, *9*, 2749−2760.
(51) Jacquemin, D.; Mennucci, B.; Adamo, C. *Phys. Chem. Chem. Phys.* **2011**, *13*, 16987−16998.
(52) Improta, R.; Scalmani, G.; Frisch, M. J.; Barone, V. *J. Chem. Phys.* **2007**, *127*, 74504.